Desalination 519 (2022) 115311

Contents lists available at ScienceDirect

Desalination

journal homepage: www.elsevier.com/locate/desal

Potentialities of thermal responsive polymer in forward osmosis (FO) process for water desalination

Rosemary Colciaghi, Riccardo Simonetti *, Luca Molinaroli, Marco Binotti, Giampaolo Manzolini

Politecnico di Milano, Dipartimento di Energia, Via Lambruschini 4, 20156 Milano, Italy

HIGHLIGHTS

- Thermo-responsive polymers and ammonium bicarbonate were studied as DSs.
- FO membrane model is used to predict water flux and membrane performance.
- Energy consumption analysis is provided for FO plant layout.
- FO process studied shows to be energy efficient for seawater desalination.

ARTICLE INFO

Keywords:
Forward osmosis
Thermal responsive polymer
Membrane design

ABSTRACT

This work aims at assessing the technical feasibility and performances of the Forward Osmosis (FO), an emergent desalination process. Two FO processes with different draw solutions have been studied: the first one is based on Ammonium Bicarbonate (AB) and the second on poly (propylene glycol-ran-ethylene glycol) monobutyl ethers (PAGBs) with different molecular weight. The two solutes have different regeneration steps, but they adopt the same membrane separation process of the salt water. The comparison between the different processes is given in terms of recovery ratio, temperature and energy requirements. AB could be regenerated through column distillation at 99.63 °C and zeolite filter, while PAGBs could be regenerated at lower temperatures (77.2 – 83.6 °C) through gravity separation followed by a final step of nanofiltration. This study showed that PAGBs have great potential to desalinate water in an energy-efficient way, reaching minimum consumptions of 39.5 kWhth/m^3 and 0.5 kWhel/m^3, even if the water recovery is not so high (< 24%). On the contrary, AB has shown higher energy consumptions (> 3.51 kWhel/m^3, > 442 kWhth/m^3). Finally, a comparison based on energy consumptions and recovery ratio with the mature desalination technologies is provided, showing the potentialities of the process when low temperature heat is available.

1. Introduction

Water is an essential commodity for human life and countries development, but nowadays one fifth of the world population has scarce access to water resource, while another quarter has access to water but does not have the technology to make it potable [1]. Considering that 97% of the water on the Earth is salty water [2], improving and developing desalination technologies is the way forward to solve this problem. The desalination technologies could be categorized into membrane processes and thermal processes [3]: the former use selective membranes and electrical energy, while the latter are based on phase change processes that require both electrical and thermal energy. Electrodialysis (ED) and reverse osmosis (RO) belongs to the first group, while multi-stage flash distillation (MSF), multi-effect distillation (MED), and vapor compression distillation (VCD) [2,4,5] to the electric-thermal driven processes. Among the different desalination techniques, MSF, MED and RO are the most diffused covering 93% of the global installed desalination capacity [1]. Several emerging desalination technologies are investigated and under development with the aim of reducing (i) the energy consumption, (ii) the cost of desalination and of addressing environmental concerns about greenhouse gases emissions [6].Among them, Membrane Distillation (MD), Humidification-Dehumidification (HDH) [9], Forward Osmosis (FO), adsorption desalination and pervaporation could exploit the use of waste heat or low-grade heat to desalinate seawater [8]. Specifically, this work focuses

* Corresponding author.
E-mail address: riccardo.simonetti@polimi.it (R. Simonetti).

https://doi.org/10.1016/j.desal.2021.115311
Received 15 July 2021; Received in revised form 13 August 2021; Accepted 19 August 2021
Available online 8 September 2021

Nomenclature

A	Water permeability (FO), LMH bar^{-1}
A_m	Membrane active area, m^2
A_2	Second virial coefficient, L ·mol^{-1}·g^{-2}
A_3	Third virial coefficient, L^2 mol^{-1} g^{-3}
B	Solute permeability, LMH
C	Concentration , M, g/L, mol m^{-3}
c_p	Specific heat, J kg^{-1} K^{-1}
D	Diffusion coefficient, m^2 s^{-1}
D^s	Diffusion coefficient in the support layer, m^2 s^{-1}
d_h	Hydraulic diameter, m
$\dot{E}$	Electrical power, kW
E_{req}	Electrical energy request per m^3 of water produced, kWh m^{-3}
E_{eq}	Equivalent electrical energy per m^3 of water produced, kWh m^{-3}
f	Friction factor, –
h	Enthalpy, J kg^{-1}
J_w	Water flux, LMH
J_s	Reverse solute flux, g m^{-2} h^{-1}, mol m^{-2} h^{-1}
K	Solute resistivity, s m^{-1}, LMH^{-1}
k	Mass transfer coefficient, m s^{-1}, LMH
L	Length, m
L_p	Water permeability (NF), LMH bar^{-1}
m	Mass flow rate, kg/ s
MW	Molecular weight, g/ mol
n	Van't Hoff coefficient, –
P	Pressure, bar
P_{loss}	Pressure drop, bar
$\dot{Q}$	Heat duty, kW
Q_{req}	Thermal energy request per m^3 of water produced, kWh m^{-3}
q	Heat flux, W m^{-2}
R	Salt rejection, –
$\dot{R}$	Universal gas constant, bar m^{3}K^{-1} mol^{-1}
Re	Reynolds number, –
RR	Recovery ratio, –
S	Structural parameter, μm
Sh	Sherwood number, –
T	Temperature, °C, K
T_{mix}	Temperature at the inlet of the primary heat exchanger/ reboiler, °C, K
t_s	Thickness of support layer, m
v	Speed , m s^{-1}
$\dot{V}$	Volumetric flow rate, m^3 s^{-1}, L s^{-1}, L/min
X	Mass concentration, kg/ kg

Acronyms

AB	Ammonium bicarbonate
ECP	External concentration polarization
ED	Electrodialysis
FO	Forward osmosis
HDH	Humidification-dehumidification
HEX	Heat Exchanger
ICP	Internal concentration polarization
KPI	Key performance parameters
LCST	Lower critical solution temperature
MED	Multi effect distillation
MD	Membrane distillation
MSF	Multi stage flash distillation
NF	Nanofiltration
PAGB	Poly(ethylene glycol)-ran-poly(propylene glycol) monobutyl ether
PEG	Polyethylene glycol
RO	Reverse osmosis
SRSF	Specific reverse solute flux
TDS	Total dissolved solids
VCD	Vapour compression distillation

Greek letters

π	Osmotic pressure, bar
η	Efficiency, –
μ	Viscosity, mPa s
δ	Thickness of boundary layer, m
ρ	Density, kg m^{-3}
γ	Zeolite dosage, g/ L
λ	Convective heat transfer, W m^{-2} K^{-1}

Subscripts

0	initial
amb	ambient
b	Bulk
D	Draw
DS	Draw side
e	Equilibrium
F	Feed
FS	Feed side
i	Interface between active and support layer in FO membrane
in	Inlet
m	Membrane
mln	Mean logarithmic
L	Lorentz
s	Solute
p	Permeate
reg	Regeneration
w	Water
wt	Weight

on FO, because of its high potentialities in seawater desalination applications [10]. FO is driven by the osmotic pressure difference between two solutions at different concentration separated by a semipermeable membrane. In the FO process, water spontaneously permeates from the feed solution, at a lower osmotic pressure, to the draw solution, at a higher osmotic pressure, without the need of high-pressure pumps as in the case of RO with consequent lower electricity consumption of desalination [7]. The diluted draw solution then undergoes through a regeneration process that requires an energy input (electrical and/or thermal, depending on the type of draw agent selected) to extract the permeated water and to re-concentrate the draw solution for reuse [7]. In the case of seawater desalination, seawater is directly used as feed, while the draw is a generic aqueous solution of a selected solute agent. Among the research topics of FO, the identification of the best draw solute is certainly the most relevant. One of the most studied draw solutes is ammonium bicarbonate (AB, NH_4HCO_3) [8], which could be regenerated through a distillation column; the major drawback of this solution is related to the traces of ammonia in the product water due to its high solubility [9]. Moon and Lee [10] investigated the regeneration part of the AB draw solution at different pressures, and they concluded that FO consumes less equivalent electrical energy than MSF, MED and RO. A pilot FO plant using AB as draw solution reports a thermal consumption of 296 kWh/m^3 without any heat recovery and an ammonia content in the final product of 17 ppm [11]. In literature different types

of draw solutes are proposed: inorganic salts [15], magnetic nanoparticles [16], nutrient compounds [17] and metathesis precipitable salts [18]. In addition, solutes which can be thermally regenerated are under development. The main advantage of thermal regeneration is the use of low temperature or waste heat to recover the water from the draw solution with significant reduction of the desalination system energy penalty. Examples of these solutes are soluble gases [19], hydrogels [20], ionic liquids [21], switchable polarity solvents [22] and thermoresponsive copolymers [23]. Different type of regeneration processes could be used according to the properties of the selected draw agent, such as MD [24], magnetic regeneration [16], chemical precipitation [18], nanofiltration [25], RO [26], distillation [27] and gravity separation [10].Focusing on the use of thermoresponsive copolymers, they show a change in their miscibility in aqueous solution with the temperature. Indeed, when the temperature is above the lower critical solution temperature (LCST), they are immiscible in water, so they could be regenerated by simple gravity separation after being heated up, while below that temperature they are miscible in water forming a homogeneous aqueous solution that could be successfully used as draw solution in FO process. Even though the use of thermoresponsive materials as regenerable draw solutes has gained particular interest because of low temperature regeneration, a comprehensive analysis of their use for FO and the overall plant assessment is still very limited in the open literature. Several studies have proven that LCST-exhibiting materials (like glycerol-oligo(ethylene oxide)-block-oligo(butylene oxide) [28], poly (4-vinylbenzyltributylammonium hexanesulfonate) [29] and poly(N-isopropylacrylamide-co-acrylic acid) [30]) have high potential as draw agents in FO process, but the energy consumptions of the recovery step are not provided by the authors. On the other hand, using the proprietary thermoresponsive draw solute of Trevi Systems®, Ahmed et al. [10] built and analysed a lab-scale FO desalination system concluding that the overall energy requirements comprises about 35-40 kWh/m^3 of heat for regeneration and around 1 kWh/m^3 of electricity for auxiliaries operation without accounting the control system consumption. Zhao et al. [24] described a FO process based on the use of poly (sodiumstyrene-4-sulfonate-co-n-isopropylacrylamide), which could be regenerated at 50 °C through MD, having thermal consumption around 29 kWh/m^3 and electrical consumption less than 4 kWh/m^3.

The main goal of this work is (i) to model a FO plant using thermoresponsive copolymers as draw solute and (ii) to compare the obtained energy consumptions, including both heat and electricity as well as the water purity, to the reference FO process adopting the AB and with respect to the current state of art of commercially available seawater desalination technologies.

2. FO layouts

Two draw solutions and consequently, two desalination configurations are considered in this work.

The first FO plant analysed is based on the use of aqueous solution of ammonium bicarbonate NH_4HCO_3 as draw solution. AB is one of the draw solute most studied in literature, since it has a unique characteristic: at temperatures higher than 60 °C it decomposes into ammonia and carbon dioxide, which are the volatiles components, and water, which is the heavier phase [31]. The desalination layout includes the FO membrane, where freshwater permeates from the seawater to the draw solution, and a regeneration part, in which the draw solution is separated from the freshwater produced. The regeneration part comprises a preheating section, a distillation column and a filtration step. The overall plant layout is provided in Fig. 1. A pre-treatment section that comprises a feed pump, anti-scalant dosing, cartridge filters, pH sensors and temperature sensors [10] is added to protect the FO membrane.

The diluted draw solution leaving the membrane module (Pt 4) is preheated by the vapours exiting the distillation column through a Heat Exchanger (HEX) and is then injected in the distillation column (Pt 5). The feed stream inlet is at the first stage of the column. In the distillation column, AB solution decomposes into carbon dioxide, ammonia and water [18]. The vapours (Pt 8) exiting the HEX are cooled down to ambient temperature and they tend to recombine together forming AB. The liquid flow exiting the bottom of the column (Pt 6) is the produced water which is cooled down and then sent to a filtration step, as suggested by [19], where the traces of ammonia are eliminated or reduced (Pt 7) below 0.5 mg/L, which is the maximum accepted content for drinkable water according to legal standards [20,21]. The filtration step is performed with zeolite, which is a material with a complex porous matrix based on silica-alumina structure, that could purify the stream of water from ammonia [22].

The second FO plant layout investigated is based on the use of thermoresponsive copolymers as draw solutes. Thermoresponsive means that these draw solutes change their characteristics and behaviour when they undertake thermal stimuli: in particular, LCST exhibiting draw agents become immiscible in water at temperature higher than a threshold value, typically higher than the ambient temperature, so they could be separated from the water by simple gravity separation.

The FO plant layout is composed by a pre-treatment section (as in the previous case), the FO membrane, a pre-heating section of the diluted draw solution, the primary HEX, a coalescer gravity separator and a NF step. The plant layout illustrated in Fig. 2 is based on the one provided by [10].

A pre-treatment section is included to control and pre-filter the

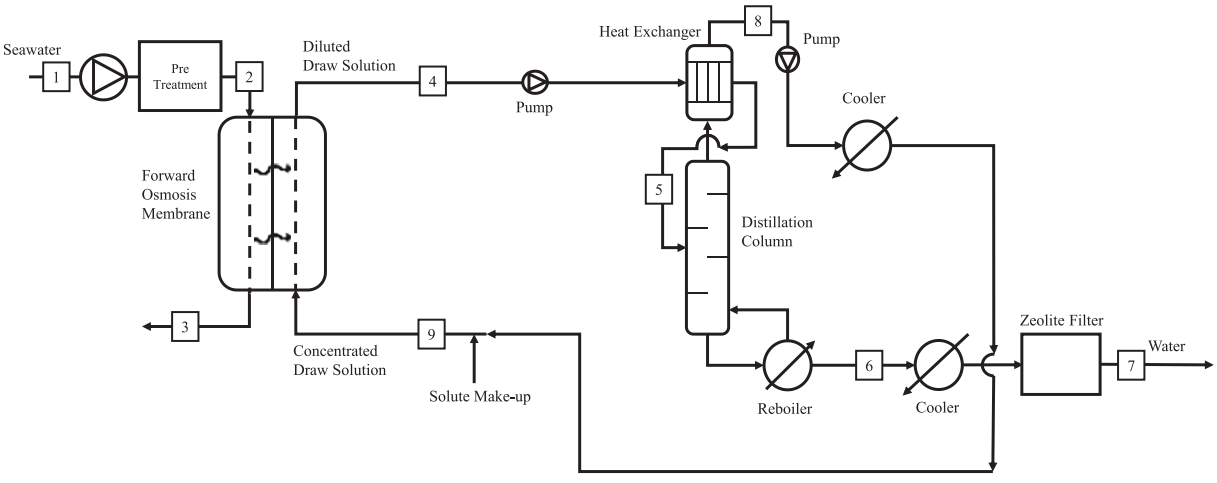

Fig. 1. Schematic diagram of the forward osmosis process based on ammonium bicarbonate as draw solute.

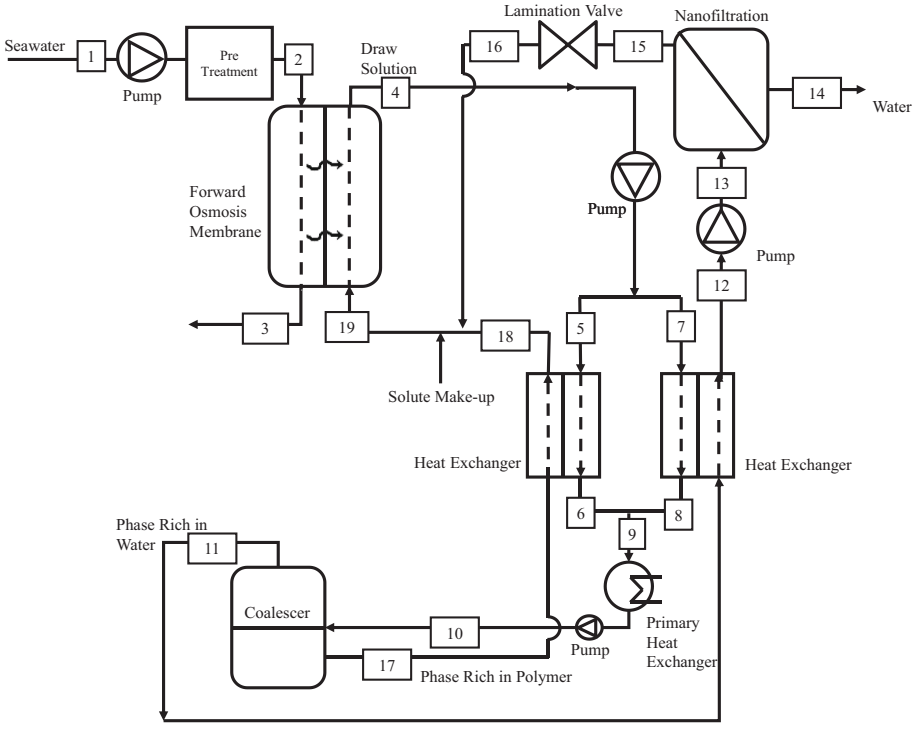

Fig. 2. Scheme of the forward osmosis plant run with thermoresponsive copolymer as draw solute, adapted from [10]. Number in labels are indicative of the points (Pt) of the process.

seawater flux, in order to protect the membrane [10]. In the FO membrane, water flux dilutes the draw solution (Pt 4), as already discussed. The diluted draw solution is then heated up in a pre-heating section, where it reaches a so-called mixing temperature (Pt 9), recovering heat from the streams at the phase separator outlet. Then, thanks to an external heat source, it reaches the regeneration temperature, at which the solute becomes immiscible in water.

The two immiscible phases are separated in a coalescer: firstly, droplets of the same material are agglomerated, becoming bigger and heavier, then a gravity separator splits the two agglomerated phases. The selected coalescer does not need any electrical or thermal energy, except for the pumping power required to overcome the pressure drop across the filter medium. After the coalescer, the two phases could be separated: the polymer-rich phase (Pt 17) is sent back to the FO membrane (Pt 19), after being cooled down by the HEX that pre-heats part of the diluting draw solution (Pt 18), while the water-rich phase (Pt 11) is cooled down in another HEX (Pt 12) that pre-heats the remaining part of the diluted draw solution and then it is sent to a Nanofiltration (NF) step (Pt 13). NF membrane stops the draw solute because of the higher molecular weight (and thus, they are larger than the NF membrane pores), permeating freshwater, that is the final distilled product (Pt 14). After NF, the flux that is not permeated is mixed with the polymer-rich phase to be re-injected in the FO membrane (Pt 16).

3. Methodology and KPIs

This section describes the methodology developed to assess the energetic performance of two different solutes, namely AB and thermoresponsive copolymers. A schematic of the methodology is provided in Fig. 3: both systems use the same FO membrane mathematical model, implemented in Matlab®, but they have two different regeneration approaches. The regeneration process for the AB includes a pre-heating section and a distillation column, modelled in AspenPlus®, and a filtration step, computed with Excel. The second system adopts three thermoresponsive polymers with different molecular weights but with the same chemical structure, whose regeneration is entirely

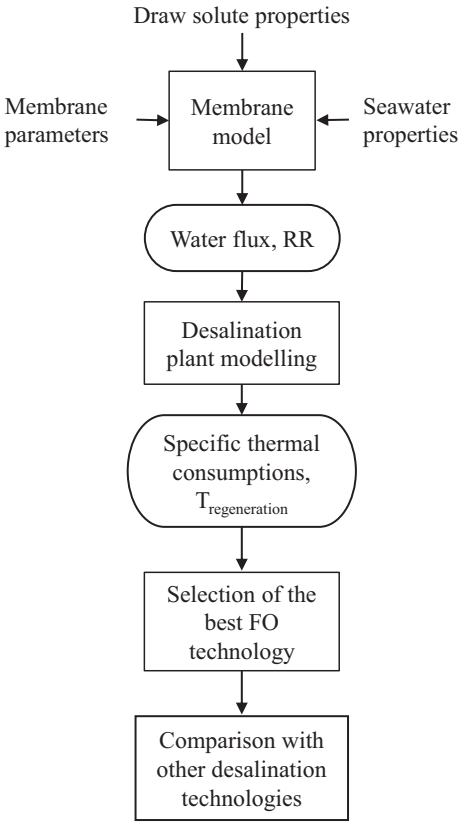

Fig. 3. Flowchart of the methodology implemented in this work.

implemented in Matlab®: it comprises pre-heating section, primary heat exchanger, a coalescer gravity separator, and a final NF step.

The performances of each layout are evaluated through key performance parameters (KPI) as the recovery ratio, the specific thermal energy consumption, specific electrical consumption and equivalent electrical consumption. Their definition is as follow.

The recovery ratio (RR) is defined as the ratio between the volumetric flow rate of water produced $\dot{V}_w$ and feed seawater that enters in the membrane $\dot{V}_{F_{in}}$ [36]:

$$RR = \frac{\dot{V}_w}{\dot{V}_{F_{in}}} \tag{1}$$

The specific thermal energy consumption represents the thermal input requested by the desalination plant $\dot{Q}$ over the rate of distilled water produced:

$$Q_{req} = \frac{\dot{Q}}{\dot{V}_w} \tag{2}$$

The specific electrical consumption is the ratio between the electrical input requested by the desalination plant $\dot{E}$ and the rate of distilled water produce, defined in a similar way of the specific thermal consumption.

$$E_{req} = \frac{\dot{E}}{\dot{V}_w} \tag{3}$$

To perform a consistent comparison accounting for the overall energy requirements between the different desalination technologies, it is used the equivalent electrical consumption. This parameter is defined as the sum of electrical and thermal consumptions, where thermal consumptions are turned into electric equivalent through Lorentz's cycle efficiency η_L:

$$E_{eq} = E_{req} + Q_{req}\eta_L \tag{4}$$

where η_L is defined as following, fixing the ambient temperature T_{amb} at 25 °C.

$$\eta_L = 1 - \frac{T_{amb}}{T_{mln}} \tag{5}$$

The mean logarithmic temperature T_{mln} is computed assuming to fix 10 °C of temperature approach to be added at the regeneration temperature T_{reg} of the draw solutions (Pt 6 and Pt 10, respectively in AB and PAGBs layout) and 5 °C of pinch point to be added at T_{mix} (Pt 5 and Pt 9, respectively in AB and PAGBs layout).

$$T_{mln} = \frac{(T_{reg} + 10°C) - (T_{mix} + 5°C)}{log\frac{(T_{reg}+10°C)}{(T_{mix}+5°C)}} \tag{6}$$

The identified KPIs are evaluated for different ranges of initial draw solution concentration.

A final comparison with other commercial technologies in terms of specific energy consumptions is provided too.

4. Forward osmosis membrane model

A 1D model of the membrane process is implemented to predict the water flux and the reverse solute flux in FO [18,19]. The asymmetric membrane has the active side facing the feed solution [37]. The dissolved solute from the draw solution permeates across the membrane in the opposite direction to the water permeation. The membrane chosen is an hollow fiber, whose geometrical characteristics are reported afterwards.

The concentration difference across the active layer of the membrane, which is the driving force of the whole process, is smaller than the bulk concentration difference between the two solutions due to concentration polarizations. Referring to Fig. 4, the water flux J_w is not proportional to the osmotic pressure difference at the bulk conditions $\Delta\pi_{ideal}$, but only to the osmotic pressure difference $\Delta\pi$ that occurs at the sides of the active layer.

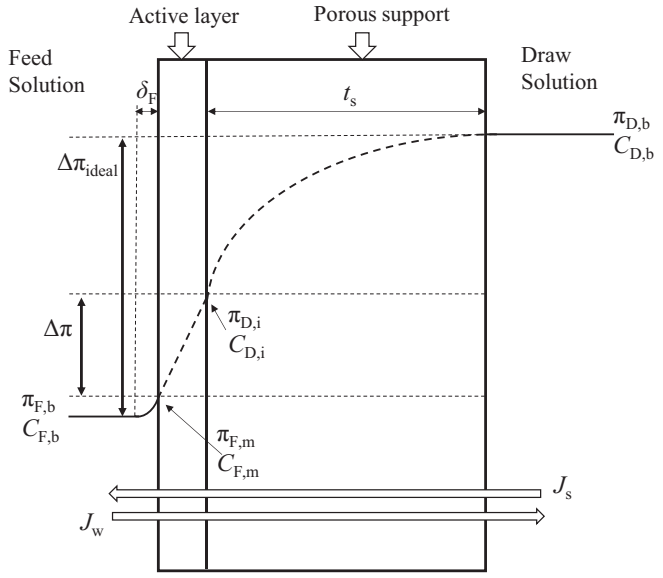

Fig. 4. Concentration profile in asymmetric membrane operating in FO mode. ICP and ECP phenomena are considered in the support layer and at the feed solution side, respectively.
Adapted from [37].

Two different concentration polarization effects can be distinguished: internal concentration polarization (ICP) and external concentration polarization (ECP), the former occurs in the support layer of the membrane, while the latter at the feed side interface. Detailed information about how ICP and ECP affect the FO performances could be found elsewhere [39,40]. Since ECP is not the main penalty in FO, it is accounted only at the feed side in this work.

About the water flux J_w across the membrane, it could be described as discussed in [40]:

$$J_w = A\,(\pi_{Di} - \pi_{Fm}) \tag{7}$$

Eq. (7) indicates that the water flux is linearly proportional to the water permeability A and the effective osmotic pressure difference across the active layer of FO membrane ($\pi_{Di} - \pi_{Fm}$), according to Fig. 4. In addition, part of the draw solute can cross the membrane, increasing the concentration of the feed side. This flux of draw solute is called reverse draw solute flux J_s, which is linearly proportional to the concentrations difference across the active layer ($C_{Di} - C_{Fm}$):

$$J_s = B\,(C_{Di} - C_{Fm}) \tag{8}$$

where B is defined as the salt permeation coefficient.

The osmotic pressure is related to the solute concentration, in particular, the Van't Hoff equation Eq. (9) could be useful to predict the osmotic pressure π for an ideal dilute solution [40], as in the case of AB solution. In Eq. (9), n is the Van't Hoff coefficient (equal to 2 in case of AB), C is the solution concentration, $\dot{R}$ is the universal gas constant and T is the solution temperature.

$$\pi = nC\dot{R}T \tag{9}$$

Only in case the Van't Hoff equation holds, the ratio between reverse solute flux and the water flux, which is called specific reverse solute flux (SRSF), could be derived as:

$$\text{SRSF} = \frac{J_s}{J_w} = \frac{B}{An\dot{R}T} \tag{10}$$

Since non-diluted and polymer solutions exhibit a nonlinear correlation between the osmotic pressure and the concentration, the Van't Hoff equation cannot be used [22]. Therefore the osmotic pressure can be expressed using the virial coefficients A_2, A_3 and the molecular weight of the solute MW_s as follows [41]:

$$\pi = C\dot{R}T\left(\frac{1}{MW_s} + A_2C + A_3C^2 + \ldots\right) \tag{11}$$

Even if the Eq. (10) could not be used for polymer solutions, as it is stated by [40], the SRSF could be considered a constant model parameter, specific for each draw solute, membrane and temperature selected. In this work, however, a conservative hypothesis is used: SRSF is supposed to be constant even at temperatures higher than the minimum one of 25 °C, in fact, since the osmotic pressure increases with the temperature, the SRSF decreases.

Following the procedure proposed by Suh and Lee [39], the draw solution concentration at the active layer interface, considering the ICP, could be expressed as:

$$C_{D_i} = \frac{C_{Db} + \frac{J_s}{J_w}}{exp\left(\frac{J_w t_s}{D^s}\right)} - \frac{J_s}{J_w} = \frac{C_{Db} + \frac{J_s}{J_w}}{exp(J_w K)} - \frac{J_s}{J_w} \tag{12}$$

where the solute resistivity for diffusion within the support layer K is defined as:

$$K = \frac{t_s}{D^s} = \frac{S}{D} \tag{13}$$

In Eq. (13) t_s is the thickness of the support layer, D^s is the diffusion coefficient in the support layer, S is the structural parameter and D is the diffusion coefficient of the draw agent in water. On the other hand, the feed solution concentration is described by [39] as:

$$C_{Fm} = \left(C_{Fb} + \frac{J_s}{J_w}\right)exp\left(\frac{J_w}{k_F}\right) - \frac{J_s}{J_w} \tag{14}$$

where the mass transfer coefficient k_F is associated to both Sherwood number Sh and hydraulic diameter d_h and can be calculated using the following equation:

$$k_F = \frac{D}{\delta_F} = \frac{Sh\,D}{d_h} \tag{15}$$

where δ_F is the thickness of the boundary layer. The Sherwood number in an hollow fiber membrane is computed through the correlations introduced by [42]. Eqs. (8) and (7) refer to local fluxes, useful to understand the mass transport phenomena in FO, but they cannot represent the concentrations and volumetric flow rates variation along the whole length of the membrane. To develop a module-scale FO process, the membrane length is discretized into N infinitesimal portions according to [38], assuming to not have cross-wound configuration. The counter-current mode, in which the two streams flow in opposite direction, is chosen since it has shown better performances than the co-current mode [43]. The mass balance along the membrane length is expressed by:

$$\frac{d\dot{V}_F}{dA_m} = \frac{d\dot{V}_D}{dA_m} = -J_w \tag{16}$$

$$\frac{d\left(C_F\dot{V}_F\right)}{dA_m} = \frac{d\left(C_D\dot{V}_D\right)}{dA_m} = J_S \tag{17}$$

where $\dot{V}_F$ and $\dot{V}_D$ are the volumetric flow rate of the feed and draw solutions, respectively and A_m represents the infinitesimal area of the membrane. These equations are solved through the finite difference method along the membrane in Matlab® environment, knowing the initial concentration and volumetric flow rate of both streams. Eq. (16) could be expressed also in terms of mass balance, considering that the density of the streams remains constant along the infinitesimal area of the membrane. A schematic representation of the discretization used in the model is provided in Fig. 5.

To evaluate the membrane performances, it is necessary to assume an initial volumetric flow rate and concentration of the draw solution at $i = 1$ (the outlet of the draw stream) and an iterative approach is adopted until convergence on $\dot{V}_D(1)$ and $C_D(1)$ is reached.

Another aspect to be taken into account is the pressure drop along the membrane. The pressure drop P_{loss} is calculated for each cell and for each stream as function of the friction factor f, the hydraulic diameter d_h and length of the channel L, the density ρ and the speed v of the solution:

$$P_{loss} = \left(f\frac{L}{d_h}\rho\frac{v^2}{2}\right) \tag{18}$$

Since in the selected cases the flow is laminar, the friction factor is calculated as [44]:

$$f = \frac{64}{Re} \tag{19}$$

In addition to the permeation, heat transfer can occur if the feed and draw solutions are at different temperature. The Soret and Dofour effects are considered negligible in this model, since it involves only binary liquid mixtures [45]. In particular, following the same nomenclature and subscripts expressed in Fig. 4, the heat flux q transferred through a membrane could be expressed as function of the global heat transfer coefficient U:

$$q = U\left(T_{Db} - T_{Fb}\right) \tag{20}$$

The expression of the energy balance of each flux in an infinitesimal element along the membrane must include the heat flux and the exchange of water flux and solute reverse flux, neglecting the temperature variation along the width W_m of the membrane (see Fig. 5), as per Eq. (21):

$$\frac{d\left(\dot{V}_F\rho_F h_F\right)}{dA_m} = \frac{d\left(\dot{V}_D\rho_D h_D\right)}{dA_m} = q - J_w\rho_w h_w + J_s\rho_s h_s \tag{21}$$

Neglecting the enthalpy h variation with the pressure, Eq. (21) becomes:

$$\frac{d\left(\dot{V}_F\rho_F c_{p_F} T_F\right)}{dA_m} = \frac{d\left(\dot{V}_D\rho_D c_{p_D} T_D\right)}{dA_m} = q - J_w\rho_w c_{p_w} T_{Fb} + J_s\rho_s c_{p_s} T_{Db} \tag{22}$$

The overall model is computed with the discretization method and finite difference method described previously. Seawater is modelled as an aqueous solution with a salt concentration of 35 g/kg and average temperature of 25 °C [46,47].

4.1. FO membrane model validation

The model developed for the description of the FO membrane is tested with membranes with known parameters and performances. Two different validations are performed to assess the use of both ionic and non-ionic draw agents.

The first membrane selected is a hollow fiber membrane presented in [48]. The process considers an aqueous solution of NaCl as draw solution and inlet volumetric flow rates of the two solutions is 30 mL/min in counter-current mode. The feed solution is deionized water. The membrane characteristics and operational parameters are reported in Table 1.

As represented in Fig. 6, the calculated water fluxes are in good accordance with the reference ones being always included in their error bars. In addition, the ratio between the reverse salt flux and the water flux is 0.14 g/L, similar to the trend line presented in [48] (see Fig. 6). Considering the relative errors of the water flux, they decrease as the draw solution concentration increase, from 13% to 4.9%. Moreover, the

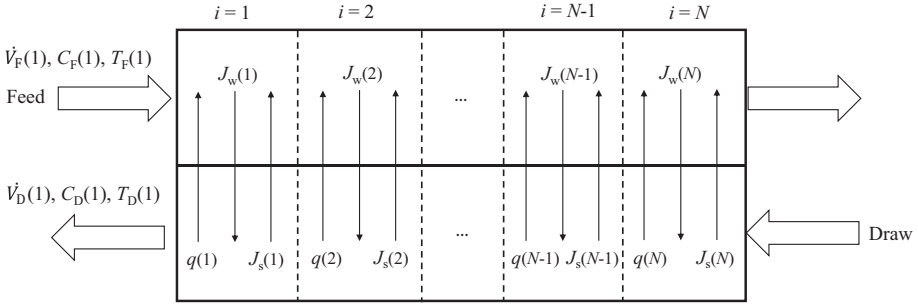

Fig. 5. Schematic of a FO module discretization operating counter-current mode. The index "*i*" represent the index of infinitesimal unit.

Table 1
Parameters and dimensions of the membranes used for the model validation [48], [40].

Parameter (case NaCl)	Value	Parameter (case glucose)	Value
Water permeability A	0.43 LMH/bar	Water permeability A	2.75 LMH/bar
Solute permeability B	0.05 LMH	SRSF	0.27 g/L
Structural parameter S	210 μm	Structural parameter	263 μm
Membrane area	116 cm^2	Membrane area	2.34 cm^2
Number of fibers	107	Membrane width	26 mm
Membrane length	210 mm	Membrane length	9 mm
Module external diameter	25.4 mm	Membrane depth	3 mm
Fiber inner diameter	300 μm		

maximum relative error in the reverse solute flux is around 12% as well.

The second membrane selected is a flat sheet membrane presented in [40] whose characteristics and operational parameters are reported in Table 1. This second process considers an aqueous solution of glucose as draw solution, which is a solute that presents a non-linear correlation between concentration and osmotic pressure. The inlet volumetric flow rates of the two solutions are 1.5 L/min and they flow in co-current mode. The feed solution is deionized water. In this case it is assumed a constant SRSF. As represented in Fig. 7, the calculated water fluxes are in good accordance with the experimental ones: the relative errors of the points considered are always lower than 6 %.

It is possible to conclude that the models used in this work can predict the experimental results, both for ionic and non-ionic draw solutes.

5. Nanofiltration membrane mathematical model

Another membrane system required by the FO desalination is the NF process. In NF, the water permeates from the concentrated solution by applying an external pressure difference to overcome the osmotic pressure difference of the two solutions, similarly to the RO. Thus, NF is a step that requires the use of a pump and consequently, electric energy. The difference between RO and NF lays on the membrane pores size: 0.1-1 nm for RO and 1-2 nm for NF [49], furthermore the maximum pressure usually involved in a NF process is 20 bar [50], while in case of RO, it could exceed 60 bar [51]. NF is one of the most newly developed liquid-phase pressure-driven membrane separation processes. It has proved to be more efficient compared with RO in many applications due to lower energy consumption and enhanced flux rates [52].

The NF membrane is here modelled as a spiral-wound membrane composed of a central permeate tube with membrane rolled around it. The membrane is supposed to be a Filmtec™ NF270-4040 [10]. To predict NF performances, a discretized cross-flow model is implemented in Matlab® environment. The membrane is modelled as a unwounded membrane neglecting the pressure variations inside the channels due to momentum change in the angular direction (see Fig. 8) [53]. To predict the performance of the module accurately, the computational domain was discretized into differential *j* lengths and *i* widths where the water flux could be calculated [54] (see Fig. 8). The water flux J_w, and pressure losses are solved at each differential area A_{cell} based on the values

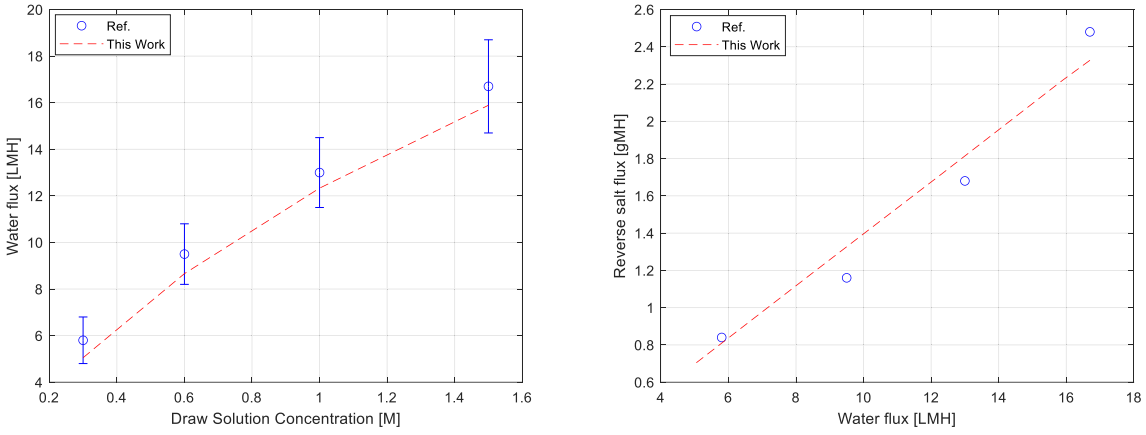

Fig. 6. Comparison of water flux and reverse salt flux between the reference's values [48] and the results of the model implemented in this work. On the left: water flux curve as function of initial draw solution concentration, on the right: reverse salt flux vs water flux.

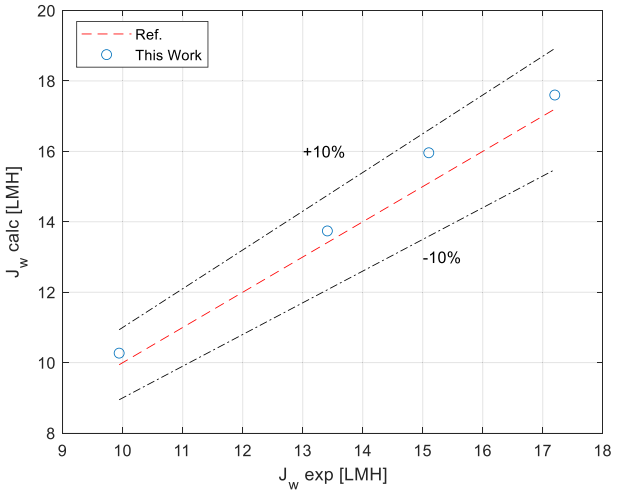

Fig. 7. Parity plot showing the distribution of experimental vs predicted values of water flux in case of glucose as draw solute of aqueous solutions at different concentrations.

entering the cell and used to update the values of the flow rate $\dot{V}$, and pressure P of the stream exiting the differential area [55].

In each discretized cell, the water flux J_w is defined as:

$$J_w = L_p(\Delta P - \Delta\pi) \tag{23}$$

where L_p is the NF membrane permeability, ΔP is the applied pressure difference and $\Delta\pi$ is the osmotic pressure difference between the two sides of the membrane, that takes into account the concentration polarization, as explained by [56].

The pressure drop P_{loss} is calculated for every cell and for each flux using Eq. (18) where the friction factor is expressed as [53]:

$$f = \frac{6.23}{Re^{0.3}} \tag{24}$$

Usually, the salt rejection R is expressed as function of the concentrations of the feed side and the permeate side [57].

$$R = 1 - \frac{C_p}{C_f} \tag{25}$$

The salt rejection could be described also through the use of the modified Peclet number and the ratio of solute Stokes radius to pore radius, as it is reported in literature [58], but in this case the ratio of solute Stokes radius to pore radius is higher than one, because the FO draw solute is bigger than the pore size, i.e. the rejection of the draw solute could be considered 100%. Moreover, this hypothesis is experimentally supported by Ahmed et al. [10], that declares that no traces of the draw solute have been found after the NF step.

5.1. NF membrane model validation

The model developed for the description of the NF membrane is tested with membrane whose parameters are described in literature.

The membrane selected is a spiral wound membrane presented in [58]. The process considers the filtration of a glucose solution at different concentrations (namely 5, 10, 50 and 100 g/L) at 50 °C. The volumetric flow rate of the feed solution is fixed at 400 L/h, and the applied external pressure varies from 4 to 28 bar. The membrane characteristics and operational parameters are reported in Table 2, and in this case the ratio of solute Stokes radius to pore radius is lower than one, that means that the rejection of the glucose is lower than 100 %.

The values of the water flux and the rejection computed with the model developed in this work are in good accordance with the reference ones (see Fig. 9): the maximum relative error of the water flux is 12 %, while the maximum relative error of the rejection is 5%.

6. Assumptions

6.1. Forward osmosis based on ammonium bicarbonate as draw solute

The process based on AB is modelled with AspenPlus® using Elec-NRTL method for streams properties and *Radfrac* as distillation column [59]. The properties of AB are retrieved from AspenPlus® database. The column considered in this system consists of 5 equilibrium stages, according to [14], it works at atmospheric pressure and it uses a kettle-type reboiler without condenser. The reboiler heat duty is set to provide a bottom product equal to the water flux permeated in the FO membrane. It is modelled considering the zeolite performance described by [60]. To model the zeolite equilibrium concentration, the Freundlich adsorption isotherm, according to [60], is selected, which is an empirical equation used to describe heterogeneous systems.

Table 2
Main parameter used for the NF membrane model validation [58].

Parameter	Value
Water permeability *Lp*	10.04 LMH/bar
Mean pore radius	0.43 nm
Ratio of solute Stokes radius to pore radius	0.842
Membrane area	40 cm^2

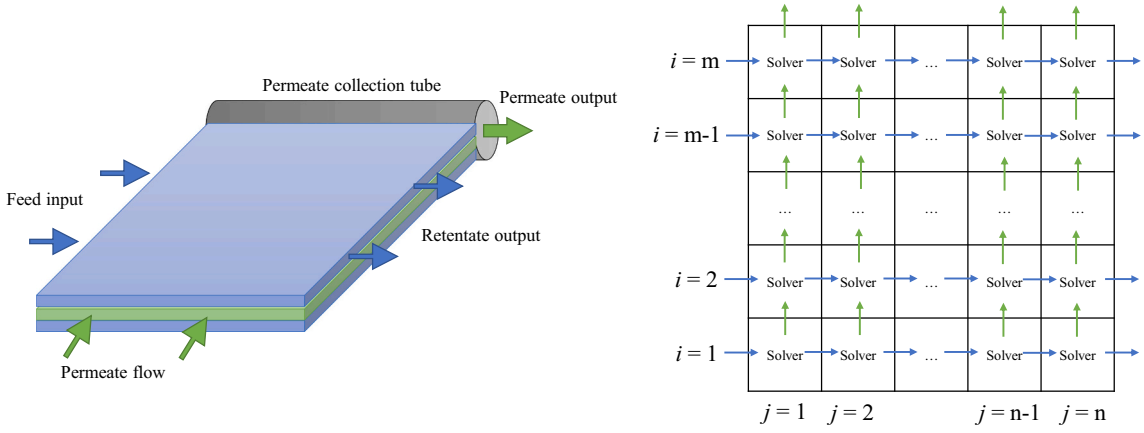

Fig. 8. On the left: schematic diagram of unwounded spiral wound leaf. On the right: discretization grid adopted in cross-flow NF model. Adapted from [53,55].

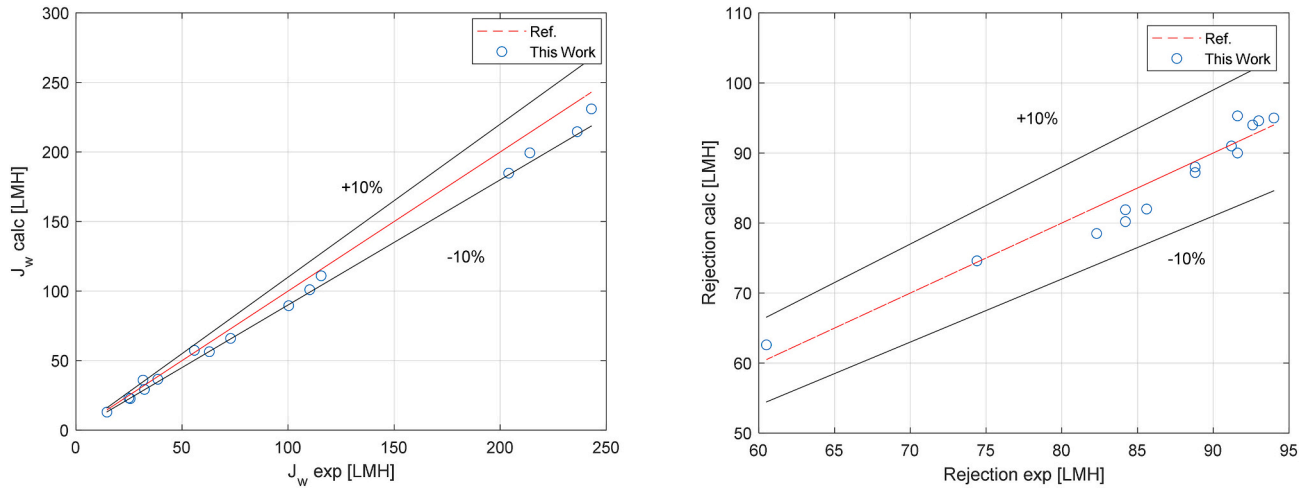

Fig. 9. On the left: parity plot showing the distribution of experimental vs predicted values of water flux in case of NF of glucose. On the right: parity plot showing the distribution of experimental vs predicted values of solute rejection in case of NF of glucose.

The electrical consumptions of the FO process include the pumps consumptions that must provide the head necessary to win the pressure drop along the different components and the cooler's auxiliaries consumptions. Further details about electrical and thermal consumptions calculations are reported in the Appendix A.2.

Since in literature it is difficult to find all the geometrical data, water permeability and structural parameter of a selected membrane, it is chosen in this work to use the FO membrane parameters based on a typical CTA membrane described in [61] (see Table 3), while the geometry is based on the Toyobo® hollow fiber-CTA membrane described in [10] (see Table 4). The geometry, A and S are the same in both AB and PAGBs case studies. The value of AB permeability in a typical CTA membrane is provided by [43]. The main plant layout assumptions are listed in Table 5.

6.2. *Forward osmosis based on thermoresponsive copolymer as draw solute*

The second layout is based on the use on copolymers called poly (ethylene glycol)-ran-poly(propylene glycol) monobutyl ether (referred as PAGB). These are copolymers composed by different segments of ethylene glycol and propylene glycol that are randomly repeated along the polymer chain; their structure is showed in Fig. 10.

Three different PAGB polymers with different molar mass are investigated: PAGB1000, PAGB2000 and PAGB4000 with a molecular weight of 1051 g/mol, 1810 g/mol and 3911 g/mol respectively. The molar volume and the specific heat of the thermoresponsive copolymers are calculated by the additive group contribution methods [58], approximating the PAGBs to Pluronics, due to the lack of more specific data in literature. Pluronics, in fact, are block copolymers that have the same ethylene oxide and propylene oxide segments of the PAGBs. With respect to PAGB, in Pluronics ethylene oxide and propylene oxide are grouped into distinct blocks. Further information about the estimation of PAGBs properties is reported in the Appendix A.1.

In this layout, the diluted draw solution is heated up in a pre-heating section and then, at the outlet of the primary HEX, it reaches the regeneration temperature of the draw agents which is 77.2 °C for PAGB2000, 83.6 °C for PAGB1000 and 80.1 °C for PAGB4000 (Pt 10),

Table 3
Main FO membrane parameters values assumed. Values of A and S are common in both AB and PAGBs cases [61], while B is expressed only for AB [43], and SRSF is expressed for thermoresponsive copolymers [41,62].

Parameter	Value
Water permeability A	0.44 LMH/bar
Structural parameter S	481 μm
Solute permeability B (AB)	0.378 LMH
SRSF (PAGB1000)	2.1 g/L
SRSF (PAGB2000)	1.2 g/L
SRSF (PAGB4000)	1 g/L

Table 4
Geometrical parameters of FO membrane.

Parameter	Value
Module external diameter	254 mm
Number of fibers	230'671
Fiber inner diameter	230 μm
Fiber external diameter	375 μm
Total active area	336 m^2

Table 5
Main components of AB plant design assumptions.

Component	Assumption	Component	Assumption
Coolers, reboiler and HEX pressure drop	0.1 bar	HEX approach	15 °C
Pump efficiency	0.85	Reboiler operating pressure	1.1 bar
Maximum pressure required by the pre-treatment pump	2 bar	Cooler auxiliary consumption per unit of heat rejected	0.8%
Zeolite dosage γ	10 g/L	Distillation column stages	5

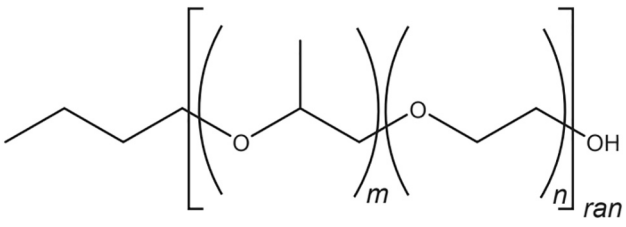

Fig. 10. General structure of poly(ethylene glycol)-ran-poly(propylene glycol) monobutyl ether. "m" represents the number of repeated units of propylene glycol, while "n" represents the number of repeated units of ethylene glycol [41].

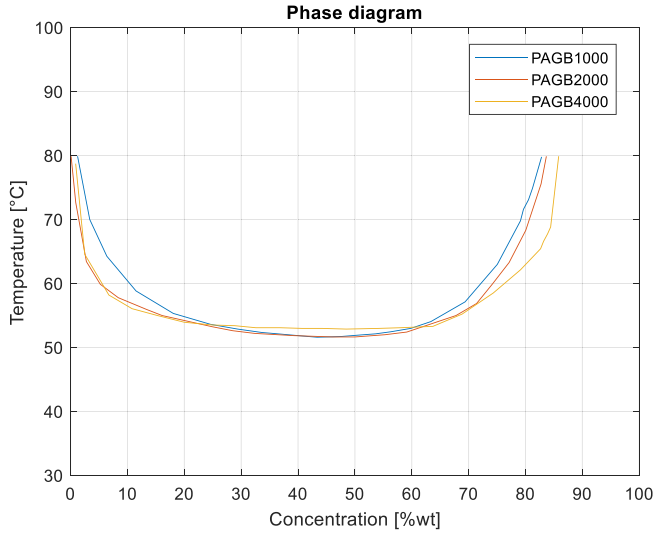

Fig. 11. Phase diagram of PAGB1000, PAGB2000, PAGB4000. Adapted from [28].

estimated through the LCST curve provided by [28] and reported in Fig. 11. At those temperatures, the diluted draw solution shows two immiscible phases: one is a polymer-rich phase, while the other is a water-rich phase. To evaluate the phase separation performed through the coalescer, the relative ratio between the polymer-rich phase and the water rich-phase is computed from the lever rule according to [64,65] using the draw solution phase diagram. The theoretical regeneration temperature is selected to fix a polymer content in the water-rich phase below 1%, according to [51], but, as stated by [7], a regeneration temperature 5 °C higher than the theoretical one must be considered due to the separation process efficiency.

The thermal consumption of the primary HEX is computed considering the mass flow rate of the diluted draw that must be heated up, and the enthalpy difference between the regeneration point (Pt 10) and the mixing point (Pt 9) that is the point where the solutions exit the two preheating sections and they are mixed before entering the primary HEX, while the electrical consumptions of the FO process are related to the pumps consumptions that must provide the head necessary to win the pressure drop along the FO membrane, pre-treatment section, HEXs, coalescer, and moreover the NF pump must provide the right pressure difference to recover drinkable water from the water-rich phase. More information about these calculations could be find in the Appendix A.2. The assumptions of the main components are reported in Table 6, while the major parameters of the membranes are provided in Table 3 and in Table 7. The FO membrane geometry, A and S are the same assumed in the AB case (see Table 4) [10,61], while the SRSF is derived from [41].

7. Results

To analyse the performances of the two configurations of FO plant, the effect of the different initial draw concentrations is firstly assessed. In particular, for AB solute the concentration varies from 0.75 M to 3.75 M (i.e. from 6 % to 37 %), to guarantee good final product quality and osmotic pressure higher than that of the seawater. For the thermoresponsive copolymer mass concentration of solute, it varies from 55 % to 80 % for each of the three polymers considered, which guarantee an osmotic pressure higher than the seawater one with limited viscosity of the draw solution. For both plants, the inlet volumetric flow rates of draw solution and feed solution are fixed respectively at 8 kg/min and 14 kg/min and the membrane module is chosen to have an effective area of 336 m^2, according to the values used by [10].

Table 6
Main components' assumptions (case PAGB layout).

Component	Assumption	Component	Assumption
HEXs pressure drop	0.1 bar	HEXs ΔT approach	10 °C
Coalescer pressure drop	1 bar	HEXs ΔT pinch point	5 °C
Maximum pressure required by the pre-treatment pump	2 bar	Pumps efficiency	0.85

Table 7
NF membrane parameters assumptions [67,68].

Parameter	Value
Water permeability L_p	14 LMH/bar
Active area	7.6 m^2

7.1. Ammonium bicarbonate as draw solution

This section discusses the results of the FO process using AB draw solute, in terms of specific thermal energy consumption, water flux and final product quality. Since different inlet draw concentrations are considered, also the volumetric flow rates in the entire plant vary, too. Table 8 provides an example of the concentration, flow rates and temperature of the process.

Water flux obtained through the membrane varies from 144 to 670 L/h for initial draw concentration from 0.75 M to 3.75 M respectively, as higher initial draw concentration entails also higher osmotic pressure difference. It could reach a recovery ratio of 80 %. However, the simulation shows that the temperature required for the regeneration is 99.63 °C for all the initial draw solution concentrations considered, which is very high and far from the 60 °C expected. This is because the decomposition of the AB starts at 60 °C but only for high concentration. However, this high value of regeneration temperature is in accordance with [13]. This high temperature is close to the one of the water evaporation and in fact, part of the water evaporates in the distillation column, increasing the heat duty. The undesired water evaporation is one of the big disadvantages of this kind of process, as also reported by [11]. Since ammonia is very soluble in water, the energy required by the reboiler for the regeneration is significant: as can be seen from Fig. 12 the lowest thermal specific consumption is around 442 kWh/m^3, corresponding to an initial draw solution concentration of 3.68 M.

The pilot plant investigated in [14] shows a thermal consumption of 296 kWh/m^3 without heat recovery, which is considerably lower than the results obtained in this simulation. However, it must be considered that the minimum ammonia content in final product was 17 ppm, which could not be accepted in drinkable water production considered in this work, where the maximum ammonia content is 0.5 ppm.

The curve of the specific thermal energy consumption decreases as the initial draw concentration increases and this is because of the high water flux permeated for high draw concentration. Considering all these aspects, it seems that increasing the concentration of the draw solution

Table 8
Concentration, temperature and mass flow rate with an inlet draw concentration at 3 M. Numbers refer to Fig. 1.

Pt	X [kg/kg]	T [°C]	m [kg/s]	Note
1	0.035	25	0.233	Seawater intake
2	0.035	25	0.233	Seawater after pre-treatment
3	0.15	35	0.056	Seawater outlet
4	0.121	26.2	0.31	Diluted draw solution
5	0.121	82.1	0.31	Distillation column inlet
6	$4.3{\cdot}10^{-6}$	99.6	0.177	Bottom outlet of distillation column
7	$3.5{\cdot}10^{-7}$	35	0.177	Final product after zeolite
8	0.108	35	0.133	Cooled NH_3-CO_2 vapour
9	0.283	35	0.133	Concentrated draw solution

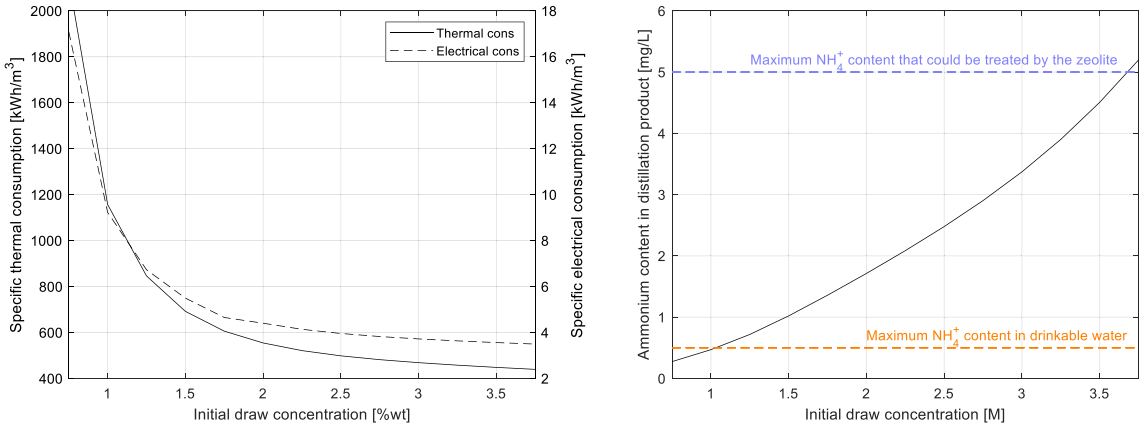

Fig. 12. On the left: specific thermal consumption (solid line) and specific electrical consumption (dashed line) of ammonium bicarbonate forward osmosis process as function of the initial molarity of the draw solution. On the right: ammonia/ammonium ion content in the product water exiting the distillation column (Pt 6).

could improve system performance, but this concentration could not be higher than 3.68 M in desalination application. In fact, as the initial draw concentration increases, also the traces of ammonia in water increases (see Fig. 12). A bottom solution ammonium concentration of 5 mg/L could be set, as the filtration step can reduce it down to 0.5 mg/L which is an acceptable ammonia content.

In Fig. 12 it is also reported the specific electrical consumptions, which are higher than 3.5 kWh/m^3. The trend of this curve is similar to the one of the thermal consumptions: it decreases as the initial draw concentration increases, since it implies higher fresh water produced. These electrical requirements involve the auxiliaries' consumptions and, specifically, the cooler auxiliaries' consumptions account for around 97% of this value. The Lorentz efficiency results to be 19.7% and the total electric equivalent consumption reaches the minimum value of 90.64 kWh/m^3.

To conclude, the best configuration is the one in which the initial draw concentration is 3.68 M, whose specific consumption is around 442 kWh/m^3 and ammonia content in the water at the outlet of the distillation column is 5 mg/L. What appeared to be very attractive by this technology was the low temperature of regeneration indicated in the literature (60 °C) but, as already said, this temperature could not be reached with the atmospheric distillation. As stated by [13], at sub-atmospheric conditions the regeneration temperature becomes lower, but then again very near to the evaporation temperature of water, which is not very convenient in desalination technologies. However, in case of vacuum distillation also the thermal consumption reduces: Boo et al. [69], calculated a thermal request of 110.3 kWh/m^3, with a final product that contains less than 1.7 mg/L of ammonia. At very high concentration of draw solute (5 or 6 M) this technology could be more advantageous, since the recovery ratio increases [31], but as we have studied in this work, the production of drinkable water using these concentrations could not be considered due to the high residues of ammonia in the final water. At high concentration in fact the water flux is higher and thus the specific energy consumption reduces, but the temperature required by the separation in any cases (also in case of vacuum distillation) are very close to the ones of the water evaporation.

7.2. Thermoresponsive copolymers as draw solution

This section presents the results of the FO process based on PAGBs. As before, different inlet draw concentrations are considered for the three different polymers studied. Table 9 provides an example of the concentrations, flow rates, temperatures and pressures. The plant is operated at atmospheric pressure, except for the NF step which operates at higher pressure but always lower than 4 bar.

The water flux ranges from 44 L/h to 184 L/h, with the higher values for higher initial draw concentration, as shown in Fig. 13. Compared to the AB case, these values are lower.

Nevertheless, the regeneration thermal requirements are good both from a temperature point of view, since the maximum solution temperature is 77.2 °C for PAGB2000, 83.6 °C for PAGB1000 and 80.1 °C for PAGB4000, and the specific consumption point of view, being in the range of 39.5 – 123 kWh/m^3 (see Fig. 13). The minimum value is in agreement with the one available in the open literature where reported thermal consumptions are around 35 – 40 kWh/m^3 [10].[1] Similarly, the

Table 9
Solute mass concentration, temperature, pressure and mass flow rates with PAGB2000 at an initial concentration of 80%$_{wt}$. Numbers refer to Fig. 2.

Pt	X[kg/kg]	T [°C]	P [bar]	m [kg/s]	Note
1	0.035	25	1	0.233	Seawater intake
2	0.035	25	1	0.233	Seawater after pre-treatment
3	0.045	30	1	0.185	Seawater outlet
4	0.587	25	1	0.182	Diluted draw solution
5	0.587	25	1.2	0.117	Diluted draw s. (inlet of pre-heating HEX, polymer-rich side)
6	0.587	67.1	1.1	0.117	Diluted draw s. (outlet of pre-heating HEX, polymer-rich side)
7	0.587	25	1.2	0.065	Diluted draw s. (inlet of pre-heating HEX, water-rich side)
8	0.587	67.1	1.1	0.065	Diluted draw s. (outlet of pre-heating HEX, water-rich side)
9	0.587	67.1	1.1	0.182	Mixed diluted draw solutions at the outlet of the HEXs
10	0.587	77.2	2	0.182	Diluted draw solution, inlet of coalescer
11	0.01	77.2	1	0.052	Water-rich phase, outlet of coalescer
12	0.01	30.4	1	0.052	Water-rich phase, outlet of pre-heating HEX
13	0.01	30.4	3.1	0.048	Water-rich phase, outlet of NF pump
14	0	30.4	1	0.052	Final product
15	0.15	30.4	3	0.004	Rejected flux from NF
16	0.15	30.4	1	0.004	Rejected flux from NF, after lamination valve
17	0.817	77.2	1	0.13	Polymer-rich phase, outlet of coalescer
18	0.817	34.7	1	0.13	Polymer-rich phase, outlet of pre-heating HEX
19	0.8	34.6	1	0.133	Concentrated draw solution

[1] This comparison is to provide an order of magnitude of the results as the draw solute is slightly different and the values *A* and *S* are not given in [7].

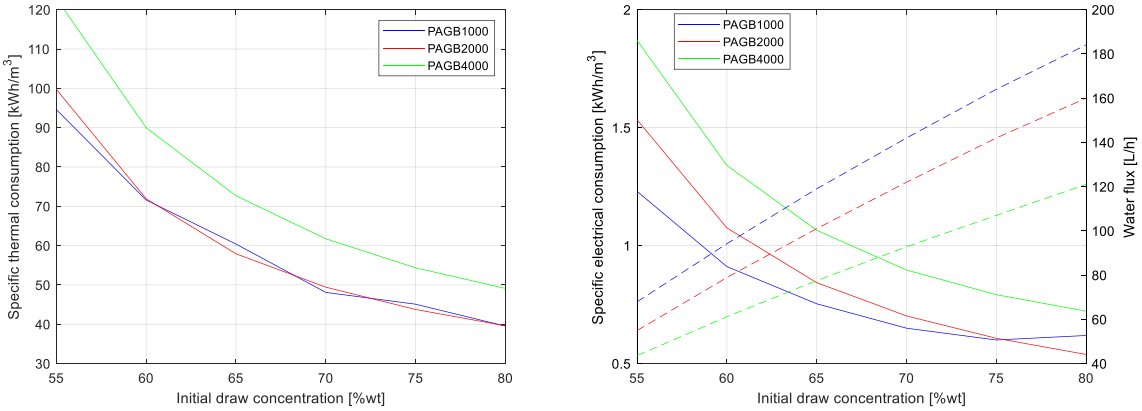

Fig. 13. On the left: Specific thermal consumption for different PAGBs draw solution, as function of initial draw concentration. On the right: specific electrical consumption (solid lines) and water flux (dashed lines) for different PAGBs draw solution, as function of initial draw concentration.

electrical requirements are very low. On the other hand, a similar FO plant based on the use of propylene glycol mono-butyl ether [70], whose regeneration temperature is fixed at 80 °C, shows that the thermal requirements of LCST-exhibiting material could be quite high (around 3000 kWh/m^3). This comparison points out that the choice of the draw solute through the family of thermoresponsive materials must consider not only the regeneration temperature of the draw solution, but also diffusivity, viscosity and other properties related to the FO membrane process.

The specific electrical consumptions are lower than 1.9 kWh/m^3. The major responsible of these consumptions is the pre-treatment, that must treat high flux of water (44 – 66% of electrical consumption), and the NF pump (9 – 27 % of electrical consumption). As the water flux permeated increases, the consumption of the NF pump increases too, because a higher flux has to flow through it. The Lorentz efficiencies are 17%, 15.5%, 16.2% respectively for PAGB1000, PAGB2000 and PAGB4000: these values are computed under the same assumptions described before, in order to estimate the total electrical equivalent consumption, that ranges from 6.7 kWh/m^3 to 21.8 kWh/m^3.

The PAGB4000 shows the lower performance, having lower water flux and higher energy consumptions. It must be considered that the diffusivity of this copolymer is lower compared to the others, leading to higher ICP. Remembering that ICP is the main causes in flux reduction, the lower trend of permeates that occurs using PAGB4000 could be easily explained [41]. PAGB2000 and PAGB1000 has very similar thermal consumptions trend. PAGB1000 has lower electrical consumptions and higher water flux, but it is penalized in the regeneration step, since it has the highest regeneration temperature among all the selected polymers (77.2 °C for PAGB2000, 83.6 °C for PAGB1000 and 80.1 °C for PAGB4000). The regeneration temperature is constant for all the initial draw solution concentrations, since it depends only on the maximum concentration set for the water-rich phase that exits the coalescer.

8. Flow rate analysis

Since the FO process based on PAGB has shown better performances in terms of energy consumptions with respect to AB, a parametric analysis with different initial mass flow rate of the feed and draw solutions is carried out. In particular, the analysis is performed considering a “base case” in which the solute selected is PAGB2000. The initial seawater flow rate and draw solution flow rate are 14 kg/min and 8 kg/min at 75% of concentration in weight, respectively.

Initially, the seawater flow rate is kept constant and equal to the one of the base case, while the initial mass flow rate of the draw solution ranges from 6 to 14 kg/min. Fig. 14 shows the recovery ratio and the specific energy consumptions trends. As the initial draw solution flow rate increases, the recovery ratio increases too, meaning that the membrane performances improve. On the other side, the thermal requirements increase with the initial draw solution flow rate and this could be due to the presence of higher water flux that has to be heated up. The specific electrical consumptions curve has a minimum in

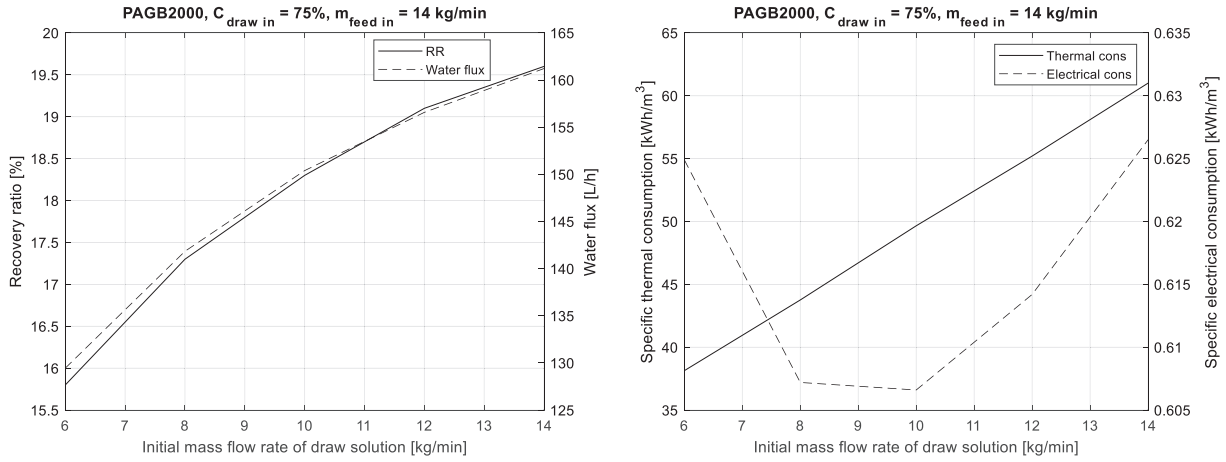

Fig. 14. On the left: recovery ratio (solid line) and water flux (dashed line) of the FO process performed at different initial mass flow rate of draw solution. On the right: specific thermal consumptions (solid line) and specific electrical consumptions (dashed line) of the FO process performed at different initial mass flow rate of draw solution.

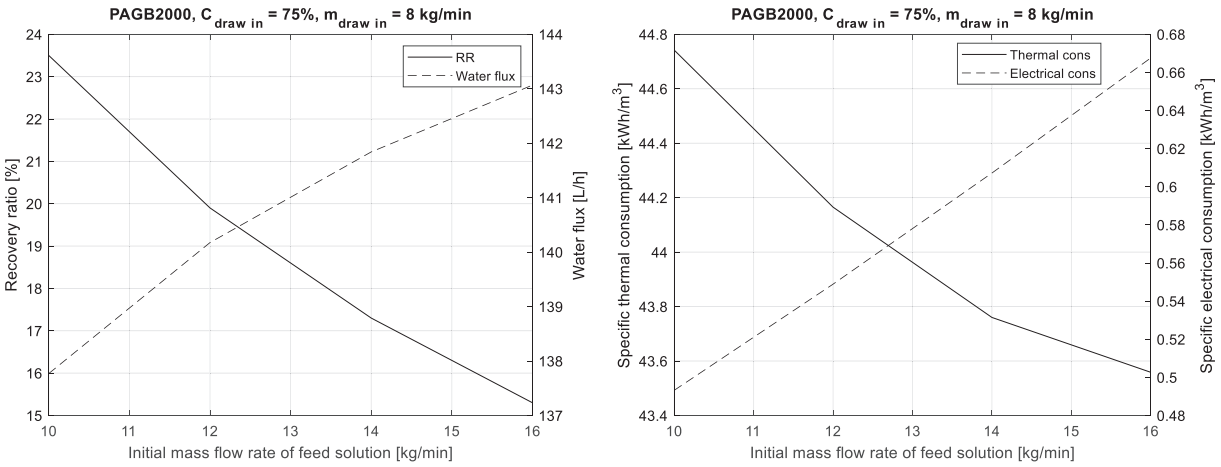

Fig. 15. On the left: recovery ratio (solid line) and water flux (dashed line) of the FO process performed at different initial mass flow rate of feed solution. On the right: specific thermal consumptions (solid line) and specific electrical consumptions (dashed line) of the FO process performed at different initial mass flow rate of feed solution.

Table 10
Characteristics of the common seawater desalination techniques [7,4] compared to the ones of the FO process studied in this work.

	MSF	MED	MVC	TVC	RO	ED	FO (PAGB)	FO (AB)
Electrical consumption [kWh_{el}/m^3]	2.5 – 5	2 – 2.5	7 – 12	1.8 – 1.6	4 – 6	2.6 – 5.5	0.5 – 1.9	> 3.51
Thermal consumption [kWh_{th}/m^3]	53 – 65	40 – 64	None	63	None	None	39.5 – 123	> 442
Equivalent electrical to thermal energy [kWh_{el}/m^3]	15.8 – 23.5	12.2 – 19.1	None	14.5	None	None	6.1 – 20	> 87
Total electricity consumption [kWh_{el}/m^3]	19.6 – 27.3	14.5 – 21.4	7 - 12	16.3	4 – 6	2.6 – 5.5	6.7 – 21.8	> 90.6
Product water quality [ppm]	≈ 10	≈10	≈ 10	≈ 10	400 – 500	150 – 500	< 150	–
Recovery ratio [%]	0.6 – 6	6 – 38	–	–	10 – 51	25 – 50	5 – 23	17 – 80

correspondence to the draw solution flow of 10 kg/min. This minimum highlights that increasing the draw flow rate, the electrical consumptions of the pumps that need to treat higher flow rates increase, but the water flux increases too. In fact, as we can see from Fig. 14 the water flux trend has an higher increase passing from 6 to 8 kg/min, resulting in reduced specific electrical consumptions.

As we can see from Fig. 14, at higher RR correspond higher thermal requirements. On the other hand, the electrical consumptions reach a minimum, thus only an economic analysis could highlight which is the best configuration. However, it could be stated that the ideal initial draw solution flow rate must be equal or lower than 10 kg/min, since at higher flow rate an increase in both electrical and thermal requirements occurs.

Then, the study focused on the effect of different initial feed flow rates. Fig. 15 shows the trend of the recovery ratio and energy requirements having fixed all the parameters to be the same as the base case, except for the feed flow rate that varies from 10 to 16 kg/min. As expected, higher feed flow rate leads to higher water flux permeated in the FO membrane thanks to the higher velocity and turbulence in the membrane, which decrease the ECP. However, since the initial feed flow rate is higher, the recovery ratio decreases. Moreover, the energy requirements trends are the opposite of the previous analysis: the thermal consumptions reduce, while the electrical consumptions increase as the feed flow rate increases. This last behaviour is expected as the higher feed flow rate, the higher electrical consumptions in the pre-treatment phase. Regarding the thermal consumptions instead, it must be considered that when the water flux increases, the diluted draw solution flow rate increases, too, leading to a growth of the heat duty requested by the primary HEX. The trend of the specific thermal consumptions highlights that even both the numerator and the denominator of the Eq. (2) increase, the water flux has an higher impact on the specific consumptions, considering that the denominator is a volumetric flow rate of pure water (whose density is lower than 1000 kg/m^3), while the numerator depends on mass flow rate of diluted draw solution.

To summarize, the variation of the draw solution flow rate has highest impact on the thermal consumptions (from -13 % up to +40 % respect to the base case), while the variation of the feed solution flow rate has highest impact on the electrical consumptions (from -19 % up to +10 % respect to the base case). However, there is a trade-off between the thermal and the electrical requirements which can be solved only by an economic analysis.

9. Comparison with other desalination technologies

Comparing the two types of solutes studied, AB reaches higher performance in terms of recovery ratio, and thus quantity of water permeated in the FO membrane. This is due to the higher water permeability of the membrane used, but also due to the lower diffusivity of the AB compared to the copolymers one, which influences the internal concentration polarization effect.

However, the membrane performance is not the main parameter that drives the choice of a draw solute. In fact, the minimization of the regeneration temperature and heat duty of the FO process is the most relevant KPIs. The regeneration temperature of the AB reaches 99.63 °C, higher than the ones of the copolymers (PAGB 1000 equal to 77.2 °C, PAGB 2000 equal to 83.6 °C and PAGB 4000 equal to 80.1 °C). Moreover, thermal consumption is very high for the AB (442 kWh/m^3) and lower for the PAGBs (39.5 – 123 kWh/m^3). Electrical consumptions are lower for the PAGBs case with respect to the AB one, too. Considering all these parameters, thermoresponsive copolymers demonstrate to be promising draw solute in FO desalination.

A comparison of the thermoresponsive copolymers-based FO with other commercial desalination seawater technologies is reported in Table 10. It results that the FO PAGB-based process has very low electrical consumptions: they are lower than the ones of the main desalination technologies, like MSF, MED, RO, ED which are higher than 1.8 kWh/m^3. Thermal requirement could reach competitive values with

respect to MED and MSF, that are in the range of 40 – 65 kWh/m^3, also considering the temperature level at which it must be provided: which is around 80 °C, a little bit higher than the one requested by the MED (< 70 °C), but less than the one requested by the MSF (90-110 °C) [3]. However, comparing the total equivalent electrical consumption with the one of electric-driven commercial desalination technologies (RO, ED), FO shows to have a higher energy request. Certainly, the utilization of waste heat for the FO process (i.e. heat rejection from power conversion cycles) could make this technology more attractive and even more competitive with respect to RO and ED. The recovery ratio ranges from 5% up to 23%, which is a good value compared to the one of the thermal desalination technologies, but quite low compared to the RO. As stated by [10], FO could reach also good quality of final water produced, with a TDS content lower than 150 ppm.

10. Conclusions

FO is an emerging desalination technology that could help to face the problem of water scarcity. The main critical aspect of this technology is related to the choice of the draw solute. Two different draw solutes and the subsequent regeneration steps are studied in this work to assess the process performance in terms of energy requirements and membrane performances. The first FO process uses AB, requiring a thermal input of around 442 kWh/m^3 at a regeneration temperature of 99.63 °C and more than 3.5 kWh/m^3 of electrical input. The second FO process is based on thermoresponsive draw solutes with LCST: it means that the aqueous solution of these solute shows two immiscible phases over a certain temperature. The process achieves good performances in terms of water recovery, quality of water and energy requirements, in fact the thermal consumptions could be as low as 39.5 kWh/m^3 and the specific electrical energy requested is always lower than 1.9 kWh/m^3. The regeneration temperature is in the range of 77.2 – 83.6 °C. This last FO technology reaches also competitive values in terms of energy request and recovery ratio with commercial thermal desalination processes MSF and MED. It reaches also lower recovery ratio than RO, but considerably lower electrical consumptions. Overall, the FO carried out using thermoresponsive copolymers seems to be a promising desalination technology in particular when coupled with heat rejection from power cycle. An interesting option consists of integrating the FO process with a concentrated solar power plant, where the waste heat from the power block could be used by the FO plant, that requires thermal energy to complete the draw agent regeneration.

Finally, the detailed process design defining optimal initial draw solution concentration and initial mass flow rate of the solutions shall be based on an economic analysis which must be considered as following step. Future research could focus on the study of other thermoresponsive draw solute that has lower temperature of regeneration.

CRediT authorship contribution statement

Rosemary Colciaghi: Methodology, Software, Validation, Writing - Original Draft, Visualization

Riccardo Simonetti: Methodology, Software, Validation, Writing - Original Draft, Visualization

Marco Binotti: Methodology, Writing - Review & Editing

Luca Molinaroli: Writing - Review & Editing, Project administration, Funding acquisition

Giampaolo Manzolini: Conceptualization, Methodology, Writing - Review & Editing, Supervision

Declaration of competing interest

The authors declare that they have no known competing financial interests or personal relationships that could have appeared to influence the work reported in this paper.

Acknowledgements

The authors would like to thank Progetti srl of Eng. Stefano Manfredi for the financial support to this research activity.

Appendix A. PAGBs properties and energy requirements

A.1. PAGBs properties estimation

Since PAGBs properties are not reported in the open literature, their values are estimated. Density and heat capacity of PAGBs solutions are computed using the lever rule between PAGBs and pure water properties, as follows:

$$\rho_{\mathrm{D}} = \rho_{\mathrm{PAGB}}\, X + \rho_{\mathrm{w}}(1 - X) \tag{A1.1}$$

$$c_{pD} = c_{p\mathrm{PAGB}}\, X + c_{p\mathrm{w}}(1 - X) \tag{A1.2}$$

The density and the heat capacity of each PAGB is computed approximating PAGBs to Pluronics, using the group contribution method presented in [63] for heat capacity and molar volume. Expression of PAGBs' densities as function of temperature is provided below, where ρ is expressed in $\frac{kg}{m^3}$ and T is expressed in °C.

$$\rho_{\mathrm{PAGB1000}} = 9.26 \times 10^{-5}\, T^4 - 0.00974\, T^3 + 0.3567\, T^2 - 6.534\, T + 1275 \tag{A1.3}$$

$$\rho_{\mathrm{PAGB2000}} = 4.088 \times 10^{-5}\, T^4 - 0.004494\, T^3 + 0.1816\, T^2 - 4.382\, T + 1233 \tag{A1.4}$$

$$\rho_{\mathrm{PAGB1000}} = 8.54 \times 10^{-5}\, T^4 - 0.008989\, T^3 + 0.3296\, T^2 - 6.079\, T + 1210 \tag{A1.5}$$

On the other hand, c_p is expressed in $\frac{J}{K\ kg}$ and T is expressed in K in the heat capacities' expressions.

$$c_{p\mathrm{PAGB1000}} = -6 \times 10^{-3} T^2 + 3.9\, T + 2347.4 \tag{A1.6}$$

$$c_{p\mathrm{PAGB2000}} = -7 \times 10^{-3} T^2 + 5.2\, T + 2158.7 \tag{A1.7}$$

$$c_{p\mathrm{PAGB4000}} = -7 \times 10^{-3} T^2 + 5\, T + 2276.3 \tag{A1.8}$$

Diffusivity of the PAGBs at 25 °C have been found in literature [41], and here are adjusted considering the temperature variation. D is expressed in $\frac{m^2}{s}$ and T is expressed in K. Although the diffusion coefficients depend on the solutes' concentrations, it was not considered for simplicity, according to

[41].

$$D_{\mathrm{PAGB1000}} = 2.22 \times 10^{-10} \frac{T}{298} \tag{A1.9}$$

$$D_{\mathrm{PAGB2000}} = 1.61 \times 10^{-10} \frac{T}{298} \tag{A1.10}$$

$$D_{\mathrm{PAGB4000}} = 1.02 \times 10^{-10} \frac{T}{298} \tag{A1.11}$$

Since in literature it is found that viscosities of PAGBs are very similar to the ones of polyethylene glycol [41], the draw solutions viscosities are estimated linearizing the results showed in [71] for polyethylene glycol (PEGs) of different molecular weight. Solutions' viscosities μ are expressed in mPa s, as function of both temperature and concentration. An example of how the viscosities of the PAGB2000 solutions are derived is provided below, where 1810 *Da* is the molecular weight of the PAGB2000, 1000 and 3350 *Da* are the molecular weights of the PEGs presented in the reference work.

$$\mu_{\mathrm{PAGB2000\ solution}} = (\mu_{\mathrm{PEG3350\ solution}} - \mu_{\mathrm{PEG1000\ solution}}) \frac{1810 - 1000}{3350 - 1000} + \mu_{\mathrm{PEG1000\ solution}} \tag{A1.12}$$

A.2. Electrical and thermal consumptions

The thermal consumptions of the AB case are provided directly by AspenPlus® in the form of heat duty of the reboiler selected. The electrical consumptions of the AB case are computed considering all the circulation pumps $\dot{E}_{\mathrm{pumps}}$, the cooler's auxiliaries' consumptions $\dot{E}_{\mathrm{cooler\ aux}}$.

$$\dot{E} = \sum \dot{E}_{\mathrm{pumps}} + \dot{E}_{\mathrm{cooler\ aux}} \tag{A2.1}$$

As already said, the cooler auxiliaries' consumptions are estimated to be 0.8% of the heat rejected, which is provided by AspenPlus®. The pumps consumptions are computed considering the head to be provided by the pump ΔP, the volumetric flow rate of the flux treated by the component $\dot{V}$ and the efficiency of the pump η_{pump}:

$$\dot{E}_{\mathrm{pump}} = \frac{\Delta P\, \dot{V}}{\eta_{\mathrm{pump}}} \tag{A2.2}$$

The thermal consumptions of the PAGB case are computed considering the mass flow rate of the diluted draw solution that exits from the FO membrane, and the enthalpy difference across the primary HEX.

$$\dot{Q} = m_{\mathrm{Pt\ 9}}(h_{\mathrm{Pt\ 10}} - h_{\mathrm{Pt\ 9}}) \tag{A2.3}$$

The electrical consumptions of the PAGB case are computed considering all the circulation pumps and the nanofiltration pump, computed following the Eq. (A2.2).

References

[1] UN OCHA, in: Water Scarcity and Humanitarian Action: Key Emerging Trends and Challenges Brief, 2010, pp. 1–15. https://www.unocha.org/es/publication/policy-briefs-studies/water-scarcity-and-humanitarian-action-key-emerging-trends-and.

[2] S. Manju, N. Sagar, Renewable energy integrated desalination : a sustainable solution to overcome future fresh-water scarcity in India, Renew. Sust. Energ. Rev. 73 (2017) 594–609, https://doi.org/10.1016/j.rser.2017.01.164.

[3] A. Al-Karaghouli, L.L. Kazmerski, Energy consumption and water production cost of conventional and renewable-energy-powered desalination processes, Renew. Sust. Energ. Rev. 24 (2013) 343–356, https://doi.org/10.1016/j.rser.2012.12.064.

[4] M.T. Ali, H.E.S. Fath, P.R. Armstrong, A comprehensive techno-economical review of indirect solar desalination, Renew. Sust. Energ. Rev. 15 (2011) 4187–4199, https://doi.org/10.1016/j.rser.2011.05.012.

[5] I. Ullah, M.G. Rasul, M.M.K. Khan, An overview of solar thermal desalination technologies, in: Latest Trends Renew. Energy Environ. Informatics, 2013, pp. 335–340.

[6] M.S. Islam, A. Sultana, A.H.M. Saadat, M.S. Islam, M. Shammi, M.K. Uddin, Desalination technologies for developing countries: a review, J. Sci. Res. 10 (2018) 77–97, https://doi.org/10.3329/jsr.v10i1.33179.

[7] M. Ali, M. El Haj, E. Taha, B. Soudan, Recent progress in the use of renewable energy sources to power water desalination plants, Desalination 435 (2018) 97–113, https://doi.org/10.1016/j.desal.2017.11.018.

[8] A. Subramani, J.G. Jacangelo, Emerging desalination technologies for water treatment: a critical review, Water Res. 75 (2015) 164–187, https://doi.org/10.1016/j.watres.2015.02.032.

[9] P. Gabrielli, M. Gazzani, N. Novati, L. Sutter, R. Simonetti, L. Molinaroli, G. Manzolini, M. Mazzotti, Combined water desalination and electricity generation through a humidification-dehumidification process integrated with photovoltaic-thermal modules: design, performance analysis and techno-economic assessment, Energy Convers. Manag. X 1 (2019), 100004, https://doi.org/10.1016/j.ecmx.2019.100004.

[10] M. Ahmed, R. Kumar, B. Garudachari, J.P. Thomas, Performance evaluation of a thermoresponsive polyelectrolyte draw solution in a pilot scale forward osmosis seawater desalination system, Desalination 452 (2019) 132–140, https://doi.org/10.1016/j.desal.2018.11.013.

[11] Y. Cai, X.M. Hu, A critical review on draw solutes development for forward osmosis, Desalination 391 (2016) 16–29, https://doi.org/10.1016/j.desal.2016.03.021.

[13] A.S. Moon, M. Lee, Energy consumption in forward osmosis desalination compared to other desalination techniques, Int. J. Chem. Mol. Nucl. Mater. Metall. Eng. 6 (2012) 421–423.

[14] Y. Kim, J.H. Lee, Y.C. Kim, K.H. Lee, I.S. Park, S.J. Park, Operation and simulation of pilot-scale forward osmosis desalination with ammonium bicarbonate, Chem. Eng. Res. Des. 94 (2015) 390–395, https://doi.org/10.1016/j.cherd.2014.08.015.

[15] A. Achilli, T.Y. Cath, A.E. Childress, Selection of inorganic-based draw solutions for forward osmosis applications, J. Memb. Sci. 364 (2010) 233–241, https://doi.org/10.1016/j.memsci.2010.08.010.

[16] Q. Zhao, N. Chen, D. Zhao, X. Lu, Thermoresponsive magnetic nanoparticles for seawater desalination, ACS Appl. Mater. Interfaces 5 (2013) 11453–11461, https://doi.org/10.1021/am403719s.

[17] J. Su, T. Chung, B.J. Helmer, J.S. De Wit, Enhanced double-skinned FO membranes with inner dense layer for wastewater treatment and macromolecule recycle using sucrose as draw solute, J. Memb. Sci. 396 (2012) 92–100, https://doi.org/10.1016/j.memsci.2012.01.001.

[18] R. Alnaizy, A. Aidan, M. Qasim, Copper sulfate as draw solute in forward osmosis desalination, J. Environ. Chem. Eng. 1 (2013) 424–430, https://doi.org/10.1016/j.jece.2013.06.005.

[19] A.A. Monjezi, H.B. Mahood, A.N. Campbell, Regeneration of dimethyl ether as a draw solute in forward osmosis by utilising thermal energy from a solar pond, Desalination 415 (2017) 104–114, https://doi.org/10.1016/j.desal.2017.03.034.

[20] J. Wang, S. Gao, J. Tian, F. Cui, W. Shi, Recent developments and future challenges of hydrogels as draw solutes in forward osmosis process, Water (Switzerland) 12 (2020) 1–20, https://doi.org/10.3390/w12030692.

[21] Y. Cai, W. Shen, J. Wei, T.H. Chong, R. Wang, W.B. Krantz, A.G. Fane, X. Hu, Energy-efficient desalination by forward osmosis using responsive ionic liquid draw solutes, Environ. Sci. Water Res. Technol. 1 (2015) 341–347, https://doi.org/10.1039/c4ew00073k.

[22] M.L. Stone, C. Rae, F.F. Stewart, A.D. Wilson, Switchable polarity solvents as draw solutes for forward osmosis, Desalination 312 (2013) 124–129, https://doi.org/10.1016/j.desal.2012.07.034.
[23] Q. Long, Y. Jia, J. Li, J. Yang, F. Liu, J. Zheng, B. Yu, Recent advance on draw solutes development in forward osmosis, Processes 6 (2018) 7–11, https://doi.org/10.3390/pr6090165.
[24] D. Zhao, P. Wang, Q. Zhao, N. Chen, X. Lu, Thermoresponsive copolymer-based draw solution for seawater desalination in a combined process of forward osmosis and membrane distillation, Desalination 348 (2014) 26–32, https://doi.org/10.1016/j.desal.2014.06.009.
[25] M. Giagnorio, F. Ricceri, M. Tagliabue, L. Zaninetta, A. Tiraferri, Hybrid forward osmosis-nanofiltration for wastewater reuse: system design, Membranes (Basel) 9 (2019) 8–12, https://doi.org/10.3390/membranes9050061.
[26] A. Al-Zuhairi, A.A. Merdaw, S. Al-Aibi, M. Hamdan, P. Nicoll, A.A. Monjezi, S. Al-ASwad, H.B. Mahood, M. Aryafar, A.O. Sharif, Forward osmosis desalination from laboratory to market, Water Sci. Technol. Water Supply 15 (2015) 834–844, https://doi.org/10.2166/ws.2015.038.
[27] R.L. McGinnis, N.T. Hancock, M.S. Nowosielski-Slepowron, G.D. McGurgan, Pilot demonstration of the NH3/CO2 forward osmosis desalination process on high salinity brines, Desalination 312 (2013) 67–74, https://doi.org/10.1016/j.desal.2012.11.032.
[28] A. Inada, K. Yumiya, T. Takahashi, K. Kumagai, Y. Hashizume, H. Matsuyama, Development of thermoresponsive star oligomers with a glycerol backbone as the draw solute in forward osmosis process, J. Memb. Sci. 574 (2019) 147–153, https://doi.org/10.1016/j.memsci.2018.12.067.
[29] C. Ju, C. Park, T. Kim, S. Kang, H. Kang, Thermo-responsive draw solute for forward osmosis process; poly(ionic liquid) having lower critical solution temperature characteristics, RSC Adv. (2019) 29493–29501, https://doi.org/10.1039/c9ra04020j.
[30] Y. Wang, H. Yu, R. Xie, K. Zhao, X. Ju, W. Wang, Z. Liu, L. Chu, An easily recoverable thermo-sensitive polyelectrolyte as draw agent for forward osmosis process, Chin. J. Chem. Eng. 24 (2016) 86–93, https://doi.org/10.1016/j.cjche.2015.11.015.
[31] J.R. McCutcheon, R.L. McGinnis, M. Elimelech, A novel ammonia-carbon dioxide forward (direct) osmosis desalination process, Desalination 174 (2005) 1–11, https://doi.org/10.1016/j.desal.2004.11.002.
[36] D.H. Furuwaka, Desalination process and technologies, Sep. Consult. Inc., United States Am. (n.d.).
[37] J.R. McCutcheon, M. Elimelech, Influence of concentrative and dilutive internal concentration polarization on flux behavior in forward osmosis, J. Memb. Sci. 284 (2006) 237–247, https://doi.org/10.1016/j.memsci.2006.07.049.
[38] A. Deshmukh, N.Y. Yip, S. Lin, M. Elimelech, Desalination by forward osmosis: identifying performance limiting parameters through module-scale modeling, J. Memb. Sci. 491 (2015) 159–167, https://doi.org/10.1016/j.memsci.2015.03.080.
[39] C. Suh, S. Lee, Modeling reverse draw solute flux in forward osmosis with external concentration polarization in both sides of the draw and feed solution, J. Memb. Sci. 427 (2013) 365–374, https://doi.org/10.1016/j.memsci.2012.08.033.
[40] H. Ryu, A. Mushtaq, E. Park, K. Kim, Y.K. Chang, J.I. Han, Dynamical modeling of water flux in forward osmosis with multistage operation and sensitivity analysis of model parameters, Water (Switzerland) 12 (2020), https://doi.org/10.3390/w12010031.
[41] A. Inada, K. Kumagai, H. Matsuyama, Effect of the molecular weights of thermoresponsive polyalkylene glycol draw solutes on forward osmosis performance, Sep. Purif. Technol. 252 (2020), 117462, https://doi.org/10.1016/j.seppur.2020.117462.
[42] S.A. Hashemifard, A.F. Ismail, T. Matsuura, M.R. Dashtarzhandi, Performance of silicon rubber coated polyetherimide hollow fibers for CO2 removal via a membrane contactor, RSC Adv. 5 (2015) 48442–48455, https://doi.org/10.1039/c5ra00085h.
[43] A. Sagiv, A. Zhu, P.D. Christofides, Y. Cohen, R. Semiat, Analysis of forward osmosis desalination via two-dimensional FEM model, J. Memb. Sci. 464 (2014) 161–172, https://doi.org/10.1016/j.memsci.2014.04.001.
[44] L. Zeghadnia, J.L. Robert, B. Achour, Explicit solutions for turbulent flow friction factor: a review, assessment and approaches classification, Ain Shams Eng. J. 10 (2019) 243–252, https://doi.org/10.1016/j.asej.2018.10.007.
[45] M. Lucke, S. Hollinger, Influence of the dufour effect on convection in binary gas mixtures, Phys. Rev. E 52 (1995) 642–657.
[46] K.G. Nayar, M.H. Sharqawy, L.D. Banchik, J.H. Lienhard, Thermophysical properties of seawater: a review and new correlations that include pressure dependence, Desalination 390 (2016) 1–24, https://doi.org/10.1016/j.desal.2016.02.024.
[47] Lenntech, Composition of seawater, (n.d.). https://www.lenntech.com/composition-seawater.htm (accessed October 4, 2020).
[48] J. Ren, J.R. McCutcheon, A new commercial biomimetic hollow fiber membrane for forward osmosis, Desalination 442 (2018) 44–50, https://doi.org/10.1016/j.desal.2018.04.015.
[49] Z. Yang, Y. Zhou, Z. Feng, X. Rui, T. Zhang, Z. Zhang, A review on reverse osmosis and nanofiltration membranes for water purification, Polymers (Basel) 11 (2019) 1–22, https://doi.org/10.3390/polym11081252.
[50] C. Charcosset, Some perspectives, in: Membr. Process. Biotechnol. Pharm, 2012, pp. 295–321, https://doi.org/10.1016/b978-0-444-56334-7.00008-3.
[51] A.J. Schunke, G.A. Hernandez Herrera, L. Padhye, T.-A. Berry, Energy recovery in SWRO desalination: current status and new possibilities, Front. Sustain. Cities. 2 (2020) 1–7, https://doi.org/10.3389/frsc.2020.00009.
[52] M.M. Zerafat, M. Shariati-niassar, S.J. Hashemi, S. Sabbaghi, A.F. Ismail, T. Matsuura, Mathematical modeling of nanofiltration for concentrated electrolyte solutions, DES 320 (2013) 17–23, https://doi.org/10.1016/j.desal.2013.04.015.
[53] Y. Roy, M.H. Sharqawy, J.H.L. V, Modeling nanofiltration for large scale desalination applications modeling of flat-sheet and spiral-wound nanofiltration configurations and its application in seawater nanofiltration, J. Memb. Sci. 493 (2016) 360–372, https://doi.org/10.1016/j.memsci.2015.06.030.
[54] S. Senthilmurugan, A. Ahluwalia, S.K. Gupta, in: Modeling of a Spiral-wound Module and Estimation of Model Parameters Using Numerical Techniques 173, 2005, pp. 269–286.
[55] Z.M. Binger, A. Achilli, Forward osmosis and pressure retarded osmosis process modeling for integration with seawater reverse osmosis desalination, Desalination 491 (2020), 114583, https://doi.org/10.1016/j.desal.2020.114583.
[56] R. Wang, Y. Li, J. Wang, G. You, C. Cai, B.H. Chen, Modeling the permeate flux and rejection of nanofiltration membrane separation with high concentration uncharged aqueous solutions, Desalination 299 (2012) 44–49, https://doi.org/10.1016/j.desal.2012.05.014.
[57] W.R. Bowen, J.S. Welfoot, Modelling the performance of membrane nanofiltration-critical assessment and model development, Chem. Eng. Sci. 57 (2002) 1121–1137, https://doi.org/10.1016/S0009-2509(01)00413-4.
[58] J.E. Almazán, E.M. Romero-Dondiz, V.B. Rajal, E.F. Castro-Vidaurre, Nanofiltration of glucose: analysis of parameters and membrane characterization, Chem. Eng. Res. Des. 94 (2015) 485–493, https://doi.org/10.1016/j.cherd.2014.09.005.
[59] T. woo Kim, Y. Kim, C. Yun, H. Jang, W. Kim, S. Park, Systematic approach for draw solute selection and optimal system design for forward osmosis desalination, Desalination 284 (2012) 253–260, https://doi.org/10.1016/j.desal.2011.09.008.
[60] M. Zhang, H. Zhang, D. Xu, L. Han, D. Niu, B. Tian, J. Zhang, L. Zhang, W. Wu, Removal of ammonium from aqueous solutions using zeolite synthesized from fly ash by a fusion method, Desalination 271 (2011) 111–121, https://doi.org/10.1016/j.desal.2010.12.021.
[61] W.A. Phillip, J.S. Yong, M. Elimelech, Reverse draw solute permeation in forward osmosis: modeling and experiments, Environ. Sci. Technol. 44 (2010) 5170–5176, https://doi.org/10.1021/es100901n.
[62] M. Giagnorio, A. Casasso, A. Tiraferri, Environmental sustainability of forward osmosis: the role of draw solute and its management, Environ. Int. 152 (2021), 106498, https://doi.org/10.1016/j.envint.2021.106498.
[63] S. Senkow, S.K. Mehta, G. Douhéret, A.H. Roux, G. Roux-Desgranges, Aqueous solutions of some amphiphilic poly(ethylene oxide)-poly (propylene oxide)-poly (ethylene oxide) triblock copolymers. a thermodynamic study over a wide concentration range at temperatures between 288.15 and 328.15 K, Phys. Chem. Chem. Phys. 4 (2002) 4472–4480, https://doi.org/10.1039/b204404h.
[64] J.P. Erikson, Partially miscible water - triethylamine solutions and their temperature dependence, J. Chem. Educ. (2016) 6–9, https://doi.org/10.1021/acs.jchemed.6b00489.
[65] D. Nakayama, Y. Mok, M. Noh, J. Park, S. Kang, Y. Lee, Lower critical solution temperature (LCST) phase separation of glycol ethers for forward osmotic control, Phys. Chem. Chem. Phys. 16 (2014) 5319–5325, https://doi.org/10.1039/c3cp55467h.
[67] Dupont, FilmTec TM Membranes. https://www.dupont.com/content/dam/dupont/amer/us/en/water-solutions/public/documents/en/45-D01529-en.pdf, 2020.
[68] A. Imbrogno, A.I. Schäfer, Comparative study of nanofiltration membrane characterization devices of different dimension and configuration (cross flow and dead end), J. Memb. Sci. 585 (2019) 67–80, https://doi.org/10.1016/j.memsci.2019.04.035.
[69] C. Boo, Y.F. Khalil, M. Elimelech, Performance evaluation of trimethylamine-carbon dioxide thermolytic draw solution for engineered osmosis, J. Memb. Sci. 473 (2015) 302–309, https://doi.org/10.1016/j.memsci.2014.09.026.
[70] L.M. Zeng, M.Y. Du, X.L. Wang, A thermodynamical approach for evaluating energy consumption of the forward osmosis process using various draw solutes, Water (Switzerland) 9 (2017), https://doi.org/10.3390/w9030189.
[71] P. González-Tello, F. Camacho, G. Blázquez, Density and viscosity of concentrated aqueous solutions of PEG, J. Chem. Eng. Data 8000 (1994) 611–614.